GUIDED ULTRASOUND WAVE PROPAGATION IN HEALING LONG BONES

V.C. Protopappas* and D.I Fotiadis**

* Dept. of Medical Physics, Medical School, University of Ioannina, GR 45 110 Ioannina, Greece
**Unit of Medical Technology and Intelligent Information Systems, Dept. of Computer Science, University of Ioannina, GR 45 110 Ioannina, Greece.

me00642@cc.uoi.gr; fotiadis@cs.uoi.gr

Abstract: In this work, we address guided ultrasound wave propagation in healing long bones. We developed a two-dimensional model of a bone-mimicking plate in which the healing process was simulated as a 7-stage process. Guided wave modes were represented in the time-frequency domain of the signal by incorporating the Lamb wave theory. The smoothed-pseudo Wigner-Ville distribution function was employed. For the intact plate, we found that the S2, A3, and S1 Lamb modes were the dominant waves for a broadband 1-MHz excitation. For the simulated healing process, we found that the S2 mode remained the dominant wave and was gradually restored during the consolidation of callus. The sensitivity of guided waves to both the structural and mechanical properties of callus can supplement velocity measurements so as to enhance the monitoring capabilities of ultrasonic evaluation.

Introduction

The ultrasonic testing of bone has been used in the assessment of metabolic diseases and the evaluation of fracture healing. The so-called axial transmission technique has been suitable to examining long bones, such as the tibia and radius. A set of transmitters and receivers is placed percutaneously (i.e. on the skin) above the region of interest [1-9] or implanted into the region [10]. The velocity of ultrasound propagation is determined by the transit time of the first-arriving signal (FAS) at the receiver.

Animal [1,2,10] and clinical studies [3,4] have showed that the propagation velocity through fractured bones increases during the healing process and when bony union is achieved, the velocity has returned to 80% the velocity through the contralateral intact bone. Experiments on fractured acrylic plates [5,6] have been carried out to examine the effect of soft tissue thickness, cortical thickness and fracture gap width on the FAS velocity.

Recent studies have demonstrated that when the wavelength is comparable to or smaller than the cortical thickness, the FAS corresponds to a lateral (or head) wave propagating along the subsurface of bone at the bulk velocity. Therefore, the velocity determined by the FAS wave is an apparent value that provides information only about a periosteal bone region. When the wavelength is comparable to or greater than the cortical thickness, the tubular bone geometry acts as a waveguide supporting the generation of additional waves.

Guided waves have gained great interest in the assessment of osteoporosis. A practical approach for representing guided waves in bones has been the use of the Lamb wave theory. Two-dimensional (2D) simulations on bone-mimicking plates [7,9], as well as *in vitro* [8] and *in vivo* experiments [9] have been carried out in order to represent and detect the two lowest Lamb modes. Ultrasound signals were recorded at various transmitter-receiver distances which were then used to produce a gray-scale mapped distance-time *(r,t)* diagram. Extraction of morphological features from the *(r,t)* diagram [9] or the application of the 2D Fast Fourier Transform [7,8] made possible the determination of the velocity of the individual modes. Although the abovementioned works have provided an improved means of characterizing healthy and osteoporotic bones, no research has focused on guided wave propagation in healing bones.

The objective of this work is to address ultrasound propagation in healing long bones. We develop a 2D bone model which also incorporates a model for callus. Callus development and maturation is simulated as a 7-stage process. Representation of theoretically predicted Lamb modes is accomplished using time-frequency signal analysis techniques. The effect of callus properties on the dispersion of guided modes is investigated. The ability of guided modes to supplement traditional FAS velocity measurements in order to enhance the ultrasonic monitoring of the healing process is demonstrated.

The Free Plate Problem

In the case of a homogeneous isotropic elastic plate with traction-free upper and lower surfaces (free plate), Lamb waves are plane strain waves [11] resulting from multiple reflections at the plate surfaces and mode conversion between longitudinal and shear waves. Lamb waves are dispersive, i.e. the velocity at which a wave propagates within a plate is a function of frequency and plate thickness. Their dispersion is described by the Rayleigh-Lamb frequency relation:

ISSN: 1727-1983

$$\frac{\tan \beta d/2}{\tan \alpha d/2} = \left\{ -\frac{4\alpha\beta k^2}{(k^2-\beta^2)^2} \right\}^{\pm 1}, \qquad (1)$$

where d is the plate thickness, $k = \omega/c$ is the wavenumber, ω is the circular frequency, c is the phase velocity of the Lamb wave, $\alpha = \frac{\omega^2}{c_L^2} - k^2$, $\beta = \frac{\omega^2}{c_T^2} - k^2$, and c_L and c_T are the longitudinal and shear bulk velocities of the medium, respectively. Changing the exponent to +1 or -1, Eq. (1) yields solutions for symmetric or antisymmetric modes, respectively. Symmetric modes, denoted as S0, S1, S2, etc., are waves with motion symmetric with respect to the midplane of the plate, whereas antisymmetric modes, denoted as A0, A1, A2, etc. have motion antisymmetric to the midplane.

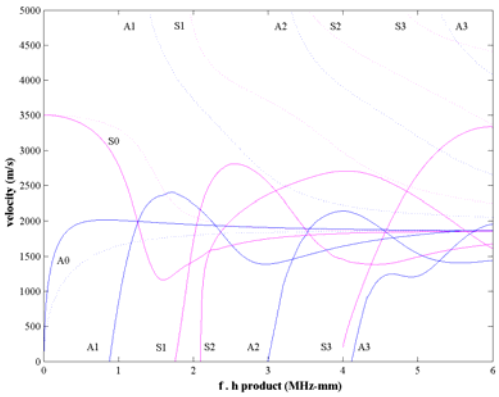

Fig. 1: The dispersion of phase (dotted lines) and group (solid lines) velocity of the first four symmetric and antisymmetric Lamb modes. The dispersion curves were calculated for a bone-mimicking plate with bulk longitudinal and shear velocity of 4063 m/s and 1846 m/s, respectively.

Solution of Eq. (1) provides with velocity dispersion curves which relate the phase velocity of a mode to the frequency-thickness product ($f \times d$). Fig. 1(a) depicts the dispersion of phase velocities of Lamb modes, whereas Fig. 1(b) the dispersion of group velocities ($c_g = \partial\omega/\partial k$). Lamb modes asymptotically approach the Rayleigh velocity for large $f \times d$, whereas for low $f \times d$ higher-order modes exhibit cut-off values. On the other hand, the two lowest modes appear all the way down to theoretical zero $f \times d$. For the latter case, the S0 mode propagates at the plate velocity, given by [11]:

$$c_{plate} = \sqrt{\frac{E}{\rho(1-\nu^2)}}, \qquad (2)$$

where E is the Young's modulus, ρ is the density and ν is the Poisson's ratio.

Materials and Methods

Bone and Callus Model

The cortex of the bone was modeled as a linear elastic isotropic plate with Young's modulus E_{bone} = 14 GPa and Poisson's ratio ν_{bone} = 0.37. Moreover, the bone was assumed to be a homogeneous solid with density ρ = 1500 kg/m^3 and plate thickness 4 mm. The selected Young's modulus, density and thickness represent average values obtained from a previous animal study [10], whereas the Poisson ratio is a typical value for bone [12]. The resulting bulk longitudinal and shear velocities of the plate were 4063 m/s and 1846 m/s, respectively.

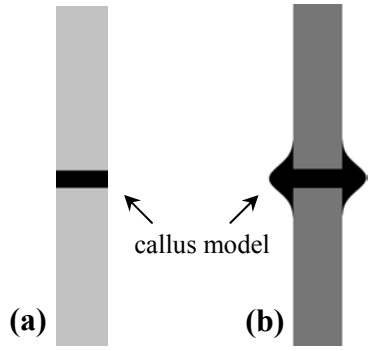

Fig. 2: The bone-mimicking plate incorporating the model of callus. In (a) the callus simply filled the fracture gap, whereas in (b) callus includes also two regions outside the plate borders.

The fracture gap was simulated by a 2-mm wide transverse discontinuity. We followed a 7-stage process to model callus formation and maturation by extending a model originally employed for studying the vibrational behavior of healing bones [12]. At each healing stage, the properties of callus were a linear combination of the properties of blood and cortical bone, according to:

$$E_{callus} = h_i \cdot E_{bone}, \qquad (3a)$$

$$\rho_{callus} = \rho_{blood} + h_i(\rho_{bone} - \rho_{blood}), \qquad (3b)$$

$$\nu_{callus} = \nu_{blood} + h_i(\nu_{bone} - \nu_{blood}), \qquad (3c)$$

where the subscript denotes the corresponding material and h_i is the i^{th} element of the vector $\langle 0, 0.01, 0.1, 0.3, 0.5, 0.7, 0.9 \rangle$ which represents a discrete healing stage. In the first healing stage, callus was modeled as non-dissipative blood which simulates the haematoma and cell proliferation that take place after a fracture. From the second stage onwards (i.e., for $i > 1$), the density and Young's modulus of callus were gradually increased, whereas its Poisson's ratio decreased. An increase in callus density and Young's modulus occurs during healing due to callus mineralization and ossification [3,13].

Furthermore, the geometry of callus evolved during healing. In the first stage, callus simply filled the fracture gap (Fig. 2(a)). From the second to the fifth stage, callus also incorporated two regions outside the plate borders. The regions were described by Gaussian-

ISSN: 1727-1983

like curves (Fig. 2(b)). In the second and third stages, the height and width of each region was 3 mm and 7 mm, respectively. In the fourth and fifth stages, the height was reduced to 2 mm, while the width was kept constant. In the last two stages, the geometry of callus was not taken into consideration as in the first stage.

Axial-Transmission

The transducers were placed perpendicular to and in contact with the plate's upper surface. The contact area of the transducer was 5 mm. The center-to-center distance of the transducers ranged from 20 – 35 mm by progressively shifting the receiver in 0.5-mm steps. The distance between the center of the transmitter and the middle of the fracture gap was 15 mm. The source wave was a broadband pulse (duration 1 μs) consisting of a single-cycle Gaussian-modulated 1-MHz sine.

Boundary Conditions

We assume that the plate was free. We defined absorbing elements at the left and right sides of the plate in order to avoid interference from reflections at the sides of the plate.

Simulation of 2D ultrasound propagation was performed with the use of a commercial software based on Finite Differences (Wave2000 Pro, CyberLogic, Inc., New York, USA). The size of the grid elements corresponded to 30 elements per shortest wavelength. The time step in the simulation, automatically set by the software, yielded a sampling frequency of 90-MHz. The duration of the signals was 110 μs.

Ultrasound Signal Analysis in the Time Domain

The criterion for determining the FAS was a threshold set at 10% of the amplitude of the first signal extremum. Such a criterion minimizes erroneous detection of the FAS as opposed to other criteria such as constant thresholds, zero-crossings, etc., which are affected by frequency-dependent attenuation and mode interference [7,9,10].

Analysis in the Time-Frequency Domain

The t-f representation of a signal resolves the energy density of various frequency components at given time-points [14]. T-f analysis has previously been employed in studying velocity dispersion of laser-generated Lamb waves in non-destructive applications of flaw detection in aluminum and composite plates [15,16].

We selected the smoothed-pseudo Wigner-Ville energy (SPWV) distribution. The t-f representation of the SPWV is [14]:

$$SPWV(t,f) = \iiint e^{i2\pi v(u-t)} G(v)h(\tau)g(v,\tau)\cdot x^*\left(u-\frac{\tau}{2}\right)x\left(u+\frac{\tau}{2}\right)e^{-i2\pi f\tau}\,dv\,du\,d\tau \quad , \qquad (4)$$

where $x^*(t)$ is the complex conjugate of the signal, $G(v)$ is a frequency-smoothing window and $h(\tau)$ is a time-smoothing window. We used Hamming $N/10$ long windows, where N is the length of the signal. We kept only the first 102.4 μs of each recording and we down-sampled to 40 MHz, which resulted in $N = 4096$ for all signals.

In order to identify the Lamb modes in the t-f domain, we used the group velocity dispersion curves. For each transmitter-receiver distance, the theoretical arrival time of each mode was calculated as a function of frequency. The dispersion curves were then superimposed on the corresponding t-f plane. The characterization of each Lamb mode was quantified by calculating the energy of the mode. This was achieved by tracing the energy density along the corresponding dispersion curve using bilinear interpolation.

Results

The signal waveform obtained from the intact plate case for 30-mm separation between the transmitter and receiver is shown in Fig. 3(a). The waveform consisted of the FAS (depicted by an arrow in Fig. 3), which is a fast low-amplitude wave, and additional higher-amplitude wave modes that arrive later at the receiver.

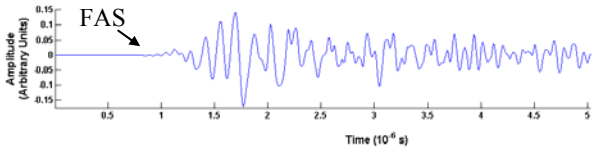

Fig. 3: The simulated signal waveform obtained from the intact plate at a 30-mm separation between the transmitter and receiver.

The propagation velocity of the FAS wave in the intact plate was calculated by the slope of the line that plots the transducers' separation against the FAS transition time. The slope was 4028 m/s (R^2 was 1.00, where R^2 is the determination coefficient from linear regression analysis) which was close to the bulk longitudinal velocity of the plate (4063 m/s) and larger than the plate velocity (c_{plate} = 3288 m/s from Eq. 2). Therefore, the FAS was not a guided mode but rather behaved as a lateral (head) wave.

The slope for each of the healing stages ranged from 4015 m/s to 4031 m/s depending on the healing stage (R^2 was 1.00). Therefore, FAS propagated as a lateral wave even in the presence of callus. The variation of the propagation velocity throughout the healing stages for 30-mm separation is illustrated in Fig. 4. At each stage, the propagation velocity was determined as the ratio of the transducers' separation to the FAS transition time. As expected, the propagation velocity increased during healing.

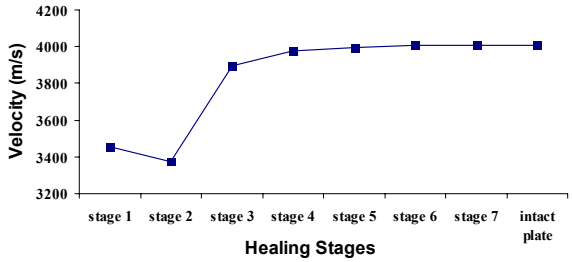

Fig. 4: The propagation velocity throughout the healing stages.

ISSN: 1727-1983

The SPWV energy distribution of a signal from the intact plate for 30-mm separation is shown in Fig. 5. The t-f representation is provided in the form of false-color images, where the color of a point represents the energy density in dB. The dispersion curves of the fist four symmetric and antisymmetric Lamb modes are also superimposed. The theoretical arrival time of each mode was calculated based on the center-to-center distance between the transducers and not on their separation.

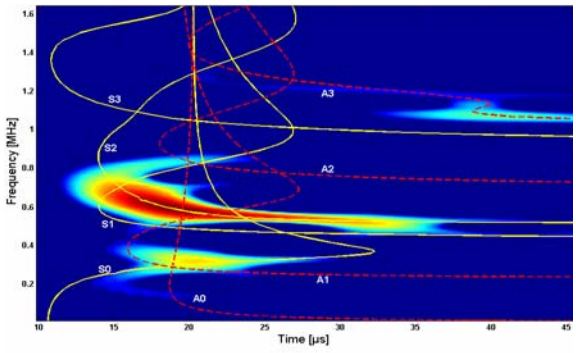

Fig. 5: The SPWV energy distributions a signal from the intact plate for 30-mm separation superimposed with the Lamb dispersions curves.

It can be observed that the S2 mode was identified from its cut-off frequency up to 0.8 MHz, the S0 mode from 0.2 – 0.35 MHz, and the A3 mode from its cut-off frequency up to 1.3 MHz. On the hand, the S1 and A1 modes were poorly characterized, while the remaining modes were not supported. With respect to the energy of each mode, the S2 was the most dominant mode followed by the A3. Mode characterization was similar for all the range of distances.

The t-f representations of the signals obtained from the fractured plate for various healing stages are shown in Fig 6. The signals contained multiple waves lying off the dispersion curves. However, the Lamb modes were gradually restored throughout the healing stages. The restoration of a Lamb mode during healing was quantified by expressing the energy of the mode at each stage as a percentage of its energy in the intact plate. The S2 mode remained the dominant wave. The restoration of the S2 mode during healing is illustrated in Fig. 7. It can be seen that the S2 mode was restored by 51% in the fifth healing stage, in which $E_{callus} = 50\% E_{bone}$, and by 100% in the sixth healing stage.

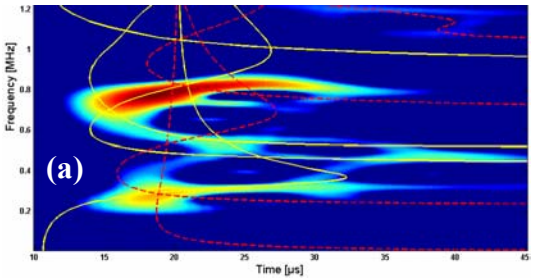

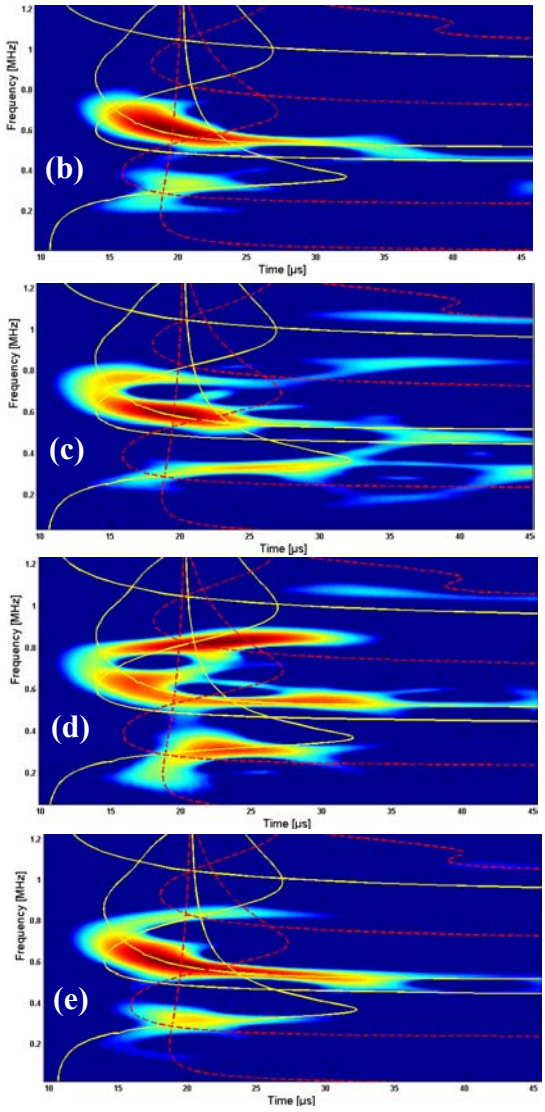

Fig. 6: The SPWV distribution of the signals from the (a) first, (b) second, (c) third, (d) fifth and (e) sixth healing stages.

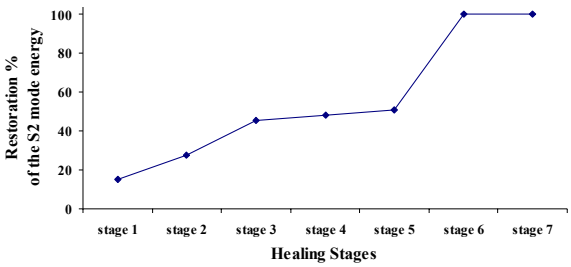

Fig. 7: The energy of the S2 mode during healing expressed as a percentage of the energy in the intact plate.

Discussion

Experiments on fractured acrylic bars as well as animal and clinical studies [1-6,10] have demonstrated the significance of ultrasound velocity measurements in determining the formation of fracture callus. In this work, we used both time and time-frequency signal

ISSN: 1727-1983

analysis techniques to address ultrasound wave propagation in healing bones.

We developed a 2D bone model similar to those reported in ultrasonic studies of osteoporosis [7,9]. We extended the model to the case of a healing tibia by incorporating a model for callus. Callus density and Young's modulus gradually increased. However, the selection for a parallel decrease in Poisson's ratio was necessary in order to achieve a smooth and realistic transition of callus bulk velocity throughout the healing stages. Nevertheless, the linearity in the relations of Eq. (3) and the association between the callus properties were selected arbitrarily. Following experimental studies [13] and the model in [12], callus dimensions were reduced during healing. However, bone and callus anisotropy, inhomogeneity and wave absorption were not taken into consideration. Moreover, the boundary conditions did not include the influence of the surrounding soft tissues. However, the assumption of a free elastic plate was necessary in order to the use the Lamb wave theory. Also, although the callus model was simple, it simulated a dynamic process and allowed the investigation of the wave propagation characteristics during healing.

The wavelength from the 1-MHz excitation was about 4-mm which was comparable to the plate thickness. It was showed that the FAS propagated in the intact plate as a lateral wave, which is in agreement with similar studies [7,9]. When callus was incorporated in the plate model, the FAS behaved again as a lateral wave. The propagation velocity, determined from the transition time of FAS, increased during healing. However, the propagation velocity offers no information about the callus geometry due to the nature of the FAS wave that is sensitive only to the periosteal region of bone.

Nevertheless, the received signals were superposed with additional wave modes that propagate throughout the bone thickness. We used a time-frequency methodology for the representation of guided modes that was recently introduced in the evaluation of engineering materials. The t-f representation of the signal from the intact plate showed that the S2 mode was the most dominant wave, whereas other modes either were identified within a specific frequency range or were not supported. Possibly, the placement of the transducers normal to plate, as opposed to through-transmission applications, did not favor the generation of some modes at specific frequencies.

In the simulated healing process, the t-f signal representations demonstrated that the properties and geometry of callus affected the theoretically predicted Lamb modes. In order to quantify the restoration of the modes during healing, we computed the energy of each mode. By comparing Figs. 4 and 7, we can observe that the restoration of the S2 mode energy was gradual and followed the consolidation of callus, whereas the restoration of the FAS velocity was almost completed when E_{callus} was only $10\%E_{bone}$. Considering that the weight-bearing capacity of a healing bone is restored when its properties have returned to 30% - 50% [3,4,13], the S2 mode can reflect callus changes within this period. Therefore, features extracted from guided wave propagation can supplement traditional velocity measurements in order to enhance the monitoring capabilities of ultrasonic evaluation.

T-f analysis has several advantages over the analysis of an *(r,t)* diagram. The acquisition of an *(r,t)* diagram requires a manual procedure and the collection of multiple and equally-spaced signals. In contrast, t-f analysis represents guided modes using only a broadband excitation. The SPWV distribution was able to represent mode dispersion; however it offers poor time-frequency resolution. The proposed t-f analysis scheme can be proved useful in other cases, such as in osteoporosis.

Conclusions

A study on the propagation of guided ultrasound propagation in simulated healing bones was presented. In the case of the intact plate, we showed that theoretically predicted Lamb waves could be represented in the t-f signal domain. Using a simulated healing process, we demonstrated that Lamb modes were gradually restored during callus consolidation. The sensitivity of mode dispersion to both callus geometrical and mechanical changes can complement traditional FAS velocity measurements and can thus improve the ultrasonic evaluation of fracture healing.

References

[1] ABENDSCHEIN W., and HAYATT G. (1972): 'Ultrasonics and Physical Properties of Healing Bone', *J. Trauma*, **12**, pp. 297-301.

[2] GILL P., KERNOHAN G., MAWHINNEY I., MOLLAN R., and MCILHAGGER R. (1989): 'Investigation of the Mechanical Properties of Bone using Ultrasound', *Proc. Inst. Mech. Eng.*, **203**, pp. 61-63.

[3] CUNNINGHAM J., KENWRIGHT J., and KERSHAW C. (1990): 'Biomechanical Measurement of Fracture Healing', *J. Med. Eng. Tech.*, **13,** pp. 92-101.

[4] GERLANC M., HADDAD D., HYATT G., LANGLOH J., and HILLAIRE P. (1975): 'Ultrasonic Study of Normal and Fractured Bone', *Clin. Orth. Relat. Res.*, **111, pp.** 175-180.

[5] LOWET G., and VAN DER PERRE G. (1996): 'Ultrasound Velocity Measurements in Long Bones: Measurement Method and Simulation of Ultrasound Wave Propagation', *J. Biomech.*, **29**, **pp.** 1255-1262.

[6] NJEH C., KEARTON J., HANS D., and BOIVIN C. (1999): 'The Use of Quantitative Ultrasound to Monitor Fracture Healing: a Feasibility Study Using Phantoms', *Med. Eng. Phys.*, **20**, pp. 781-786.

[7] BOSSY E., TALMANT M., and LAUGIER P. (2002): 'Effect of Cortical Thickness on Velocity Measurements using Ultrasonic Axial Transmission: a 2D Simulation Study', *J. Acoust. Soc. Am.*, **112**, pp. 297-307.

ISSN: 1727-1983

[8] LEFEBVRE F., DEBLOCK Y., CAMPISTRON P., AHITE D., and FABRE JJ. (2002) 'Development of a New Ultrasonic Technique for Bone and Biomaterials In Vitro Characterization', *J. Biomed. Mater. Res.*, **63**, pp. 441-446.

[9] NICHOLSON P., MOILANEN P., KARKKAINEN T., TIMONEN J., and CHENG S. (2002): 'Guided Ultrasonic Waves in Long Bones: Modeling, Experiment and In Vivo Application', *Phys. Meas.*, **23**, pp. 755-768.

[10] PROTOPAPPAS V., BAGA D., FOTIADIS D., LIKAS A., PAPACHRISTOS A., and MALIZOS K. (2005): 'An Ultrasound Wearable System for the Monitoring and Acceleration of Fracture Healing in Long bBones', *IEEE Trans. Biomed. Eng.* **52,** pp. 1597-1608.

[11] ROSE J. L. (1999): 'Ultrasonic waves in solid media', (Cambridge University Press, Cambridge).

[12] LOWET G., DAYUAN X., and VAN DER PERRE G. (1996): 'Study of the Vibrational Behaviour of a Healing Tibia Using Finite Element Modelling', *J. Biomech.*, **29**, pp. 1003-1010.

[13] DEN BOER F., BRAMER J., PATKA P., BAKKER F., BARENTSEN R., FEILZER A., DE LANGE E., and HAARMAN H. (1998); 'Quantification of fracture healing with three-dimensional computed tomography', *Arch. Orthop. Trauma. Surg.,* **117**, pp. 345-350.

[14] WILLIAMS W. (1999): 'Biological Applications and the interpretations of time-frequency signal analysis', in AKAY M. (Ed): 'Time frequency and wavelets in biomedical engineering', (IEEE Press, New York).

[15] NIETHAMMER M., JACOBS L., QU J., and JARZYNSKI J. 'Time-frequency representations of Lamb waves', *J. Acoust. Soc. Am.*, **109**, pp.1841-1847.

[16] PROSEER W,, SEALE M., and SMITH B. (1999): 'Time-frequency analysis of the dispersion of lamb modes', *J. Acoust. Soc. Am.,* **105**, pp. 2669-2676.

ISSN: 1727-1983